Journal of Engineering Science and Technology
Vol. 14, No. 6 (2019) 3234 - 3251

HEAT TRANSFER PHENOMENA OF PREMIXED AND DIFFUSION FLAMES IMPINGING ON CYLINDRICAL SURFACES

SATYANANDA TRIPATHY[1], MANMATHA K. ROUL[2,*], AKSHAYA KU. ROUT[3]

[1]School of Mechanical Engineering, KIIT University, Bhubaneswar, 751024, India
[2]Department of Mechanical Engineering, GITA, Bhubaneswar, 752054, India
[3]School of Mechanical Engineering, KIIT University, Bhubaneswar, 751024, India
*Corresponding Author: mkroul@gmail.com

Abstract

Impinging jet is a proficient method to transfer energy in many industrial applications. In the present study, numerical analysis is done for premixed and diffusion turbulent flames impinging normally on cylindrical surfaces. The objective of the present work is to investigate the influence of geometrical constraints on heat transfer characteristics. The heat flux propagation on the plane surface completely depends on the plate separation distance, Reynolds number and the Equivalence Ratio (ER). The solution of the differential equation related to conservation of momentum, mass and energy has been analysed. The radiative heat transfer model has been designed by using several radiation models and the turbulence phenomenon is analysed by the help of RNG K-ε turbulence model. In the response plot, it indicates that the heat flux increases progressively with the radial distance towards the centre of the plate to achieve the maximum value at a position a bit away from stagnation point and thereafter it reduces. In case of diffusion flame, the heat flux is more at the stagnation region as compared to a premixed flame, while the maximum heat flux remains almost identical for both premixed and diffusion cases. When the distance between the plate and the nozzle increases, the peak heat flux is very close to the stagnation point. The effect of heat transfer phenomena on equivalence ratio, Reynolds number and separation of the plate from the nozzle has been studied.

Keywords: Diffusion flame, Equivalence ratio, Nusselt number, Premixed flame.

1. Introduction

The use of jet flames has been found in several industries to achieve better heat transfer coefficient and to produce high rates of heat transfer. Heating by flames in industrial furnaces is employed to increase heat flux and thereby reduce fuel consumption significantly. The jet impingement heat transfer is a well-established research area with practical relevance in the field of heat transfer, with a good amount of contributions by several researchers.

Chander and Ray [1] used Discrete Ordinate (DO) model to simulate radiant heat transfer and found that if the length of the inside zone is smaller than the distance of the target plate from the inlet section, the maximum heat flux will increase as the Reynolds number increases. Conaro et al. [2] observed that most of the studies using collisions were performed on a plane, and the influence of the curvature of the surface of the target plate on heat transfer phenomenon has not been studied at all.

Dong et al. [3] proposed the correlation between different geometry and working parameters of Nusselt numbers. Hou and Ko [4] studied the heat transfer due to impinging flames on inclined plates and observed that the temperature and efficiency of the plate strongly depend on the distance of the target from the nozzle and the angle of inclination of the target plate. The flame structure is strongly dependent on the angle of inclination of the target plate for low heights, and for high heating heights, this effect is negligible. Kuntikana and Prabhu [5] compared the heat transfer between the premixed flame nozzle and the isothermal air injector with the variation of jet Reynolds number to the target surface, which is cooled from the opposite side.

Agrawal et al. [6] studied the effect of a turbulent flame collision on the slope and found that the heat flux distribution in the lower part of the plate increases with the angle, but slightly depends on the angle of inclination. Tripathy et al. [7] studied the theoretical diffusion and the premixed turbulent flame acting on a flat surface and found that the average Nusselt number on the plate increases as the Re and ER and *H/d* of the flame increase. Hindasageri et al. [8] investigated the experimental and numerical studies were on heat transfer from the jet to a plane target plate. They found that heat flux depends upon the separation distance. Wei et al. [9] studied experimentally the flame collision of premixed biogas with laminar flow. It was established that the total heat transfer and heat exchange rate increased significantly with the increase of unburned gas velocity. Singh et al. [10] gave the radial distribution of the flame temperature at different axial heights and other working conditions, in which, the heat transfer characteristics of compressed natural gas were studied experimentally.

Nayak et al. [11, 12] experimentally and numerically studied the natural convective heat transfer in heated vertical pipes and found the correlation between Nusselt number and Reynolds number. Sahoo et al. [13, 14], considered the natural convective heat transfer in a vertical isothermal plate having protrusions, and predicted the average number as a function of fin height, fin aspect ratio and the inclination of the fins. Roul and Dash [15, 16] investigated the effect of various turbulence models on flow characteristics. Gorji-Bandpy et al. [17] established a new process for the effectiveness of heat exchanger networks by using the genetic algorithm and chronological quadratic programming and found that the projected networks is better than traditional optimization methods. Pourmehran et al. [18]

described the principles of volumetric flow rate and distribution of pressure for incompressible lubricant flow with various conditions of variables and velocities. Rahimi-Gorji et al. [19] described that the engine performance varies significantly according to the variation of weather condition. Therefore, to optimize the output and fuel consumption, the engine must be calibrated according to the weather condition.

It appears from the review of literature that a comprehensive theoretical work is needed for a further generalized understanding of the influences of the pertinent operating parameters like burner geometry, plate separation distance, types of flame (premixed or diffusion), Reynolds number and equivalence ratio on heat transfer characteristics in both normal and oblique impingement of flame on plane and curved surfaces. The conclusive review of the literature as mentioned above provides the scope of the present work, which pertains to a thermo fluid modelling of both premixed and diffusion turbulent flames impinging normally and obliquely on a plane and curved surfaces to investigate the different aspects of flame impingement heat transfer.

2. Numerical Solution

Physical model of normal flame impingement of premixed and diffusion flames on the cylindrical surface has been shown in Figs. 1(a) and (b) respectively. Methane and air are considered to be fuels and oxidants, respectively. In case of premixed flame, the methane-air mixture flows through the cylindrical nozzle of diameter 12 mm with their initial velocities for different Reynolds numbers. However, in case of diffusion flame, there are two concentric cylindrical nozzles at the inlet, i.e., one is the outer nozzle of diameter 12 mm and other is the inner nozzle of diameter 4 mm. Air and methane flow in the outer and inner nozzle respectively with their initial velocities for different Reynolds numbers varying from 4000 to 15000. The jet Reynolds number referred to in this study is a turbulent flame. The radiative heat transfer model has been designed by considering Discrete Ordinates (DO) radiation model. The turbulence phenomena are analysed by the help of RNG K-ε turbulence model.

The boundary condition for this work can be written in a cylindrical coordinate system as follows.

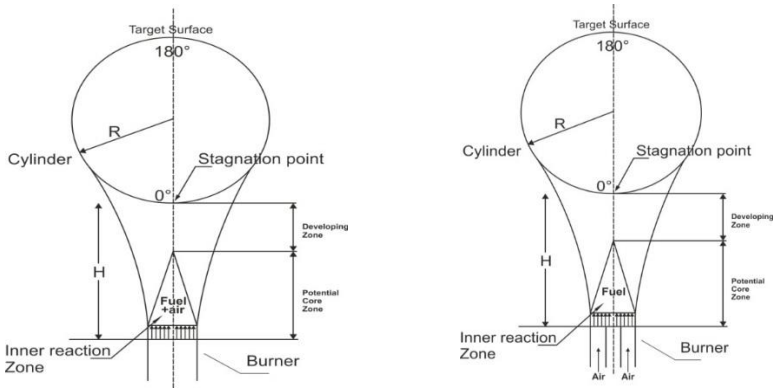

(a) Premixed flames. **(b) Diffusion flames.**

Fig. 1. Methane-air turbulent flames impinging normally on cylindrical surfaces.

In this analysis, ANSYS Fluent software is used. The finite volume method is used to solve the conservation equations for mass, momentum, energy, turbulent kinetic energy, rate of dissipation of turbulent kinetic energy. A SIMPLE algorithm is employed for pressure-velocity coupling. Secondly, order upwind scheme is used for discretizing diffusion and advection terms. The convergence criteria for the residuals in all the discretized equations were set to 10^{-6}. A number of grids along radial and axial directions were taken as 150 (r) × 60 (z) to discretize for H/d = 4. For higher H/d ratios the number of grids along z-direction was increased proportionately.

The following assumptions have been made in this study:

- The system is considered to be a grey body with respect to radiation characteristics.
- The flow is turbulent but steady and the flow at the outlet of the nozzle is considered to be uniform.
- The irreversible two steps global reaction is considered for the oxidation of methane.
- The gas-phase comprising air and products of combustion is assumed to obey the ideal gas laws.

Governing equations:

With all the above assumptions the governing equations are given by:

- Mass equation:

$$\nabla(\rho\vec{v}) = 0 \tag{1}$$

- Momentum equation:

$$\rho[\vec{v}\,\nabla\vec{v}] = -\nabla p + \nabla\left(\mu_{eff}\nabla\vec{v}\right) + \vec{F}_B \tag{2}$$

Here μ, μ_t and μ_{eff} are laminar, turbulent and effective viscosity respectively. $\vec{F}_B$ is the gravitational body force.

- Turbulent kinetic energy equation:

$$\nabla(\rho\vec{v}k) = \nabla\left(\frac{\mu_t}{\sigma_k}\nabla k\right) + G_k - \rho\varepsilon \tag{3}$$

and the rate of dissipation of turbulent kinetic energy equation

$$\nabla(\rho\vec{v}\varepsilon) = \nabla\left(\frac{\mu_t}{\sigma_\varepsilon}\nabla\varepsilon\right) + C_{1\varepsilon}\frac{\varepsilon}{k}G_k - \rho C_{2\varepsilon}\frac{\varepsilon^2}{k} \tag{4}$$

where K, ε and G_K *are t*he turbulent kinetic energy, rate of dissipation of turbulent kinetic energy and generation of turbulent kinetic energy respectively.

- Energy equation:

$$\nabla(\rho\vec{v}h) = \nabla\left(\rho\alpha_{eff}\nabla h\right) - \nabla\vec{q}^r \tag{5}$$

where $h = \sum_{k=1}^{N} Y_k\left[h_{f,k}^0 + \int_{T_{ref}}^{T} c_{p,k}\,dT\right]$

Here, h is the enthalpy of the mixture, h_f^0 is the enthalpy of formation, α_{eff} is the effective thermal diffusivity.

- Species conservation:

$$\nabla(\rho\vec{v}Y_k) = \nabla\left(\rho D_{eff}\,\nabla Y\right) + S_k \tag{6}$$

where D_{eff} is effective mass diffusivity, and S_k is the source term for k^{th} species.

- Chemical kinetics:

The equations for the oxidation of methane are given by:

$$\mathrm{CH_4} + 1.5\mathrm{O_2} = \mathrm{CO} + 2\mathrm{H_2O} \tag{7}$$

$$\mathrm{CO} + 0.5\mathrm{O_2} = \mathrm{CO_2} \tag{8}$$

The rate of reaction is given by Magnussen and Hjertager [20] as given below:

- Arrhenius equation:

$$\dot{\omega}_{fk} = B(\rho)^{a+b}\frac{Y_f^a Y_o^b}{M_f^a M_o^b} exp\left(-\frac{E}{\bar{R}T}\right) \tag{9}$$

- Magnussen and Hjertager equation:

$$\dot{\omega}_{fd} = A\frac{\rho}{M_f}\frac{\varepsilon}{k}\left[min\left(Y_f, \frac{Y_o}{\gamma}, \frac{cY_P}{1+\gamma}\right)\right] \tag{10}$$

where M and γ are the molecular weight and stoichiometric ratio respectively.

- Radiation model:

The DO (Discrite Ordinate) model is considered for radiation modelling. The radiative transport equation is given by:

$$\nabla.(I(\vec{r},\vec{s})\vec{s}) + (a+\sigma_s)I(\vec{r},\vec{s}) = an^2\frac{\sigma T^4}{\pi} + \frac{\sigma_s}{4\pi}\int_0^{4\pi} I(\vec{r},\vec{s}^t)\Phi(\vec{s}.\vec{s}^t)\,d\Omega^t \tag{11}$$

where $\vec{r}$, $\vec{s}$ and $\vec{s}^t$ are position vector, direction vector and scattering direction vector respectively. And σ_s, σ, I, φ and Ωt are scattering coefficient, Stefan-Boltzmann constant, in the intensity of radiation, phase function and solid angle respectively.

- Heat transfer coefficient:

The average heat- transfer coefficient is given by:

$$\bar{h} = \frac{1}{A}\int hdA \tag{12}$$

And local heat- transfer coefficient is written as:

$$h = \frac{q_w}{(T_{ad}-T_w)} \tag{13}$$

where T_{ad} and T_w are the adiabatic flame temperature and wall temperature respectively.

The wall heat flux q_w is written as:

$$q_w = -k\left(\frac{\partial T}{\partial z}\right)_{plate} + q_{rw} \tag{14}$$

where q_{rw} is the heat flux due to radiation at the target surface.

The heat-transfer to the plate is given by

$$Q = \int q_w \, dA \tag{15}$$

The average Nusselt number, $\bar{N}u$ is given by

$$\bar{N}u = \frac{\bar{h}(2R)}{k} \tag{16}$$

Boundary conditions and operating parameters:

Axi-symmetric boundary condition is considered along the jet axis. Therefore, r - z computational domain is taken as shown in Fig. 2.

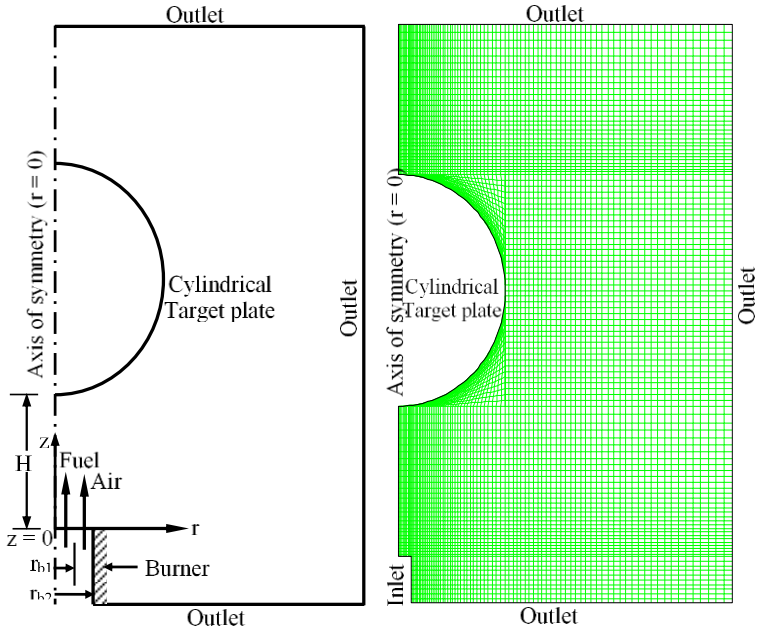

Fig. 2. Computational domain.

- At inlet (z = 0):

For premixed flame:

$$U_r = 0,\ U_z = U_i, T = T_i, Y_{CH_4} = Y_{CH_{4i}}, Y_{O_2} = Y_{O_{2i}}, where\ 0 \le r \le r_b$$

For diffusion flame:

$$U_r = 0,\ U_z = U_{if}, T = T_i, Y_{CH_4} = 1, Y_{O_2} = 0, where\ 0 \le r \le r_b$$

$$U_r = 0,\ U_z = U_{ia}, T = T_i, Y_{CH_4} = 0, Y_{O_2} = 0.23, where\ r_{b1} \le r \le r_{b2}$$

where r_{b1} refers to the inner radius and r_{b2} refers to the outer radius of the nozzle.

- At axis of symmetry (r = 0):

$U_r = 0, \frac{\partial U_z}{\partial r} = \frac{\partial T}{\partial r} = \frac{\partial \rho}{\partial r} = \frac{\partial Y_k}{\partial r} = 0$

- At target plate ($z = H$):

No slip: $U_r = 0$

No penetration: $U_z = 0$

Isothermal: $T = T_w$

Impermeable: $\frac{\partial Y_k}{\partial z} = 0$

- Outlet:

Radial direction: $\frac{\partial U_z}{\partial r} = \frac{\partial U_r}{\partial r} = \frac{\partial T}{\partial r} = \frac{\partial Y_k}{\partial r} = 0$

Axial direction: $\frac{\partial U_z}{\partial z} = \frac{\partial U_r}{\partial z} = \frac{\partial T}{\partial z} = \frac{\partial Y_k}{\partial z} = 0$

- Nozzle wall:

Adiabatic: $\left(\frac{\partial T}{\partial r}\right)_w = 0, or\ \dot{q}_w = 0$

For the numerical calculations, methane-air premixed and diffusion turbulent flame is considered. The temperature of the air and fuel at the exit plane of the burner was taken as 300 K. The distance of the target plate from the nozzle and the flow rates are changed to get different dimensionless parameters as given below:

- Reynolds number, $\text{Re} = \frac{\rho v_i d}{\mu}$: 4000, 6000, 8000, 10000, 15000
- Equivalence ratio, $\text{ER} = \frac{(Y_a/Y_f)_s}{(Y_a/Y_f)_a}$: 0.8, 1.0, 1.2, 2.0

Here, subscripts *s* and *a* are referred to stoichiometric air-fuel ratio and actual air-fuel ratio of the mixture respectively.

- The ratio of the separation distance of the target plate to the nozzle diameter, H/d = 4, 8, 12.
- The ratio of the cylinder diameter to the nozzle diameter, D/d = 4, 8, 12.

The inlet velocity of fuel and air in premixed and diffusion flame can be calculated from the relation, $\text{Re} = \frac{\rho U_i d}{\mu}$

For premixed flame:

For fuel (methane) flow:

d = 0.012 m, at 300 K the kinematic viscosity = 17.28 * 10^{-6} m^2/s ,

For Re = 4000, U_{if} = 5.7 m/s and for Re = 15000, U_{if} = 21.6 m/s

Hence, for fuel flow, the velocity at inlet varies from 5.7 m/s to 21.6 m/s for the Jet Reynolds numbers varying from 4000 to 15000.

Similarly, for air flow:

d = 0.012 m, at 300 K the kinematic viscosity = 4.765 * 10^{-5} m^2/s,

For Re = 4000, U_{ia} = 15.88 m/s and for Re = 15000, U_{ia} = 59.56 m/s.

Thus, for airflow, the velocity at inlet varies from 11.91 m/s to 59.56 m/s for the Jet Reynolds numbers varying from 4000 to 15000.

T_i is taken as 300 K.

For diffusion flame:

For inlet velocity of fuel and air:

For fuel (methane) flow:

d = 0.004 m, at 300 K the kinematic viscosity = 17.28 * 10^{-6} m^2/s ,

For Re = 4000, U_{if} = 17.28 m/s and for Re = 15000, U_{if} = 64.8 m/s

Thus, for fuel flow the velocity at inlet varies from 17.28 m/s to 64.8 m/s for the Jet Reynolds numbers varying from 4000 to 15000.

Similarly for air flow:

d = 0.008 m (hydraulic diameter), at 300 K the kinematic viscosity = 4.765×10^{-5} m^2/s,

For Re = 4000, U_{ia} = 23.82 m/s and for Re = 15000, U_{ia} = 89.34 m/s

Hence, for airflow, the velocity at inlet varies from 23.82 m/s to 89.34 m/s for the Jet Reynolds numbers varying from 4000 to 15000.

T_i is taken as 300 K.

3. Results and Discussion

In this analysis, an isothermal target plate of specified temperature is considered. The theoretical prediction of this model for the case of the premixed flame is compared with the experimental data of van der Meer [21] as illustrated in Table 1. The theoretical result of the present model matches closely with the experimental data.

Table 1. Comparison of present theoretical predictions with experimental data [21].

Fixed input parameters	**Variable parameters for both experimental (21) and present model**	**Nu (at stagnation point)**	
Fuel: Methane	***H/d***	**Experimental results [21]**	**Theoretical predictions by present model**
	2	68.25	60.20
Premixed flame	4	112.10	103.25
ER = 1.0	6	116.50	108.40
Re = 4226	8	107.90	97.30

The optimal size distribution of the numerical mesh to be used, for a given value of *H/d*, was determined from several numerical experiments, which showed that further refinements in grids in either direction did not change the results by more

than 2%. Table 2 shows the average Nusselt number as a function of a number of cells for different values of *H/d* for Re = 6000.

Figure 3 shows the variation of average Nusselt number as a function of grid size for different values of *H/d*. It can be seen from Table 2 and Fig. 3 that for *H/d* = 4, as the number of cells in the domain increase from 3000 to 9000, the average Nusselt number changes from 96.204 to 124.125. Further increase in a number of grids up to 20000 has a negligible effect on the average Nusselt number. Similarly, for *H/d* = 8, as the number of cells in the domain increases from 12000 to 36000, the average Nusselt number changes from 92.634 to 121.403. Further increase in a number of grids up to 80000 has a negligible effect on the average Nusselt number. And for *H/d* = 12, as the number of cells in the domain increases from 27000 to 81000, the average Nusselt number changes from 72.315 to 91.236. Further increase in the number of grids up to 140000 has almost no effect or negligible effect on the average Nusselt number.

Table 2. Average Nusselt number as a function of number of cells to decide grid independency.

Sl. No.	*H/d* = 4		*H/d* = 8		*H/d* = 12	
	No. of grids	Nu	No. of grids	Nu	No. of grids	Nu
1	3000	96.205	12000	92.634	27000	72.315
2	4800	130.518	19200	127.703	43200	98.123
3	7000	126.316	28000	123.214	63000	93.402
4	9000	124.125	36000	121.403	81000	91.236
5	12600	123.309	50400	120.626	113400	90.445
6	20000	122.934	80000	119.916	140000	89.762

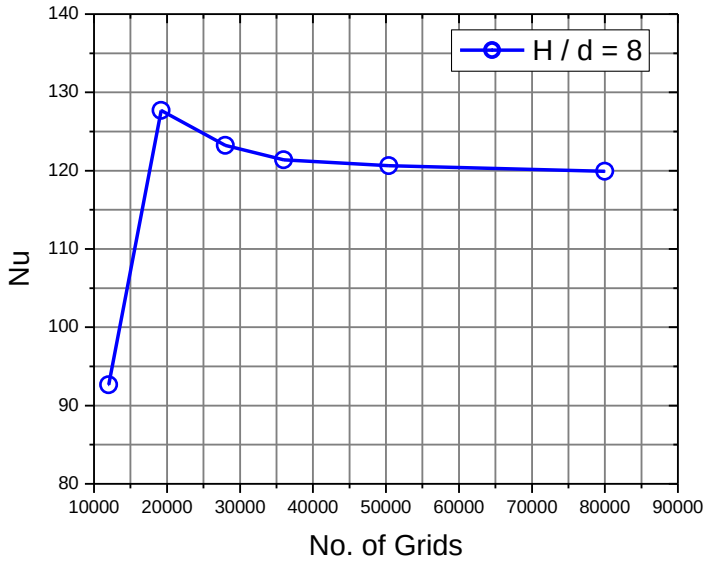

Fig. 3. Average Nusselt number as a function of grid size for *H/d* = 8.

Figure 4 represents the variations of average Nusselt number over the plane surface with Re for different values of plate separation distance at ER = 1 for premixed flame and found that with an increase in Reynolds number Re, average Nusselt number increases. It is also observed from Fig. 4 that the total heat flux from the plate for *H/d* = 4 is more than that for *H/d* = 8 up to a Reynolds number of 10000, beyond which, the trend is reversed. The reason for this may be due to the variations of typical flame shape and the resulting heat flux distribution at the plate surface for different values of Re and *H/d*. When *H/d* = 4, the plate is close to the burner and the flame is mostly attached to the plate at all Reynolds numbers. In this situation, it brings about a greater convective effect with reducing both the hydrodynamic and thermal boundary layer for the flow of hot gases past the plate surface. This results in an increase in the rate of heat transfer. When the plate is kept at a larger distance from the burner, the flame is usually attached to nozzle rim. With an increase in Re, the flame length gets increased and the high-temperature reaction zone comes closer to the plate resulting in an enhanced overall heat transfer.

Figure 5 represents the temperature field for the premixed flame of the plane surface at *H/d*=12, ER = 1 and Re = 6000. In case of *H/d* = 12, the flame looks almost like a nozzle stabilized envelop flame due to the presence of the target plate.

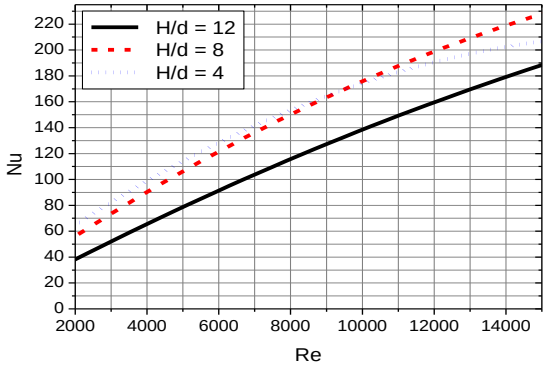

Fig. 4. Variations of $\overline{\mathrm{Nu}}$ with Re and *H/d* in premixed flames (ER = 1).

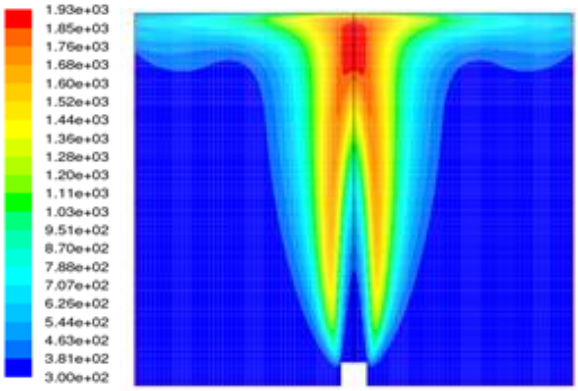

Fig. 5. Temperature profile for premixed flames of plane surface at *H/d* = 12, ER = 1, Re=6000 (temperature is in K).

This is ascribed to the radial spreading of flame and it is so shaped due to the interference of the target plate. Under this situation, there exists a short unreacted burner attached cool conical core, which is surrounded by a high-temperature flame zone that extends almost up to the plate surface. For higher values of *H/d*, the temperature of the flame is reduced due to the entrapment of more air from the surrounding.

The velocity and temperature profile in flame impingement on a cylindrical surface for specified operating conditions, i.e., D/d = 8, H/d = 8, ER =1 and Re = 6000 are shown in Figs. 6 and 7 respectively. It is evident from Fig. 6 that the velocity magnitude at $\theta = 0^0$ is around 5 m/s. As θ increases from 0^0 to 90^0 the velocity magnitude increases up to 11.6 m/s. At $\theta = 180^0$ there is recirculation of flow and the velocity decreases significantly. It can be seen from Fig. 7 that fluid temperature increases from almost 300 K at $\theta = 0^0$ to 2230 K at $\theta = 25^0$. Thereafter, there is a separation of flow from the surface. The same trend is also obtained in the velocity profile in Fig. 6.

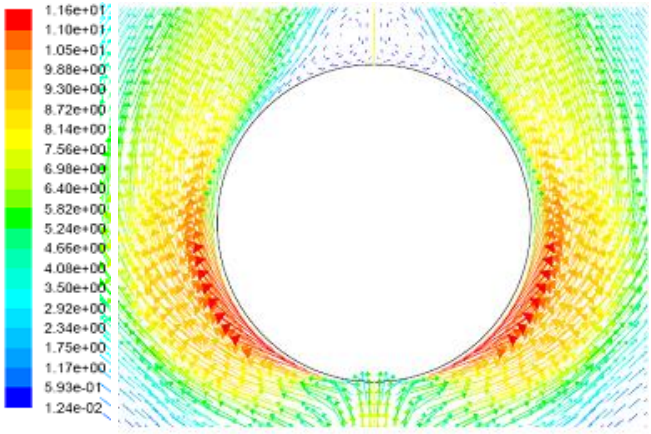

Fig. 6. Velocity profile in flame impingement on a cylindrical surface (Re = 6000, ER = 1).

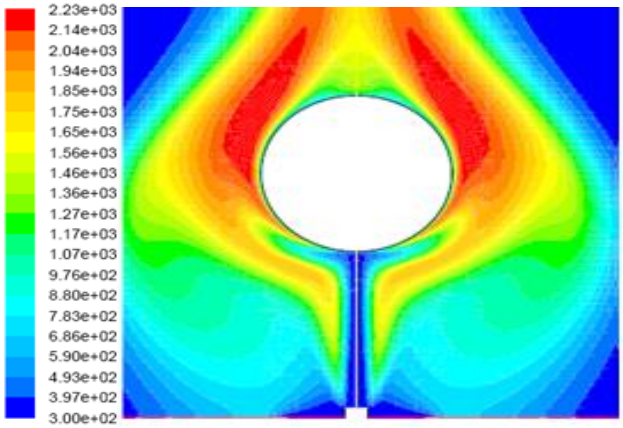

Fig. 7. Temperature profile in flame impingement on a cylindrical surface (Re = 6000, ER = 1).

In Figs. 8 and 9, the radial allocation of local heat flux for various values of *D/d* on a cylindrical surface is shown both for premixed and diffusion flame (Re = 6000 and ER = 1). In Fig. 8 for various values of cylinder diameter D the heat flux distributions are shown symmetrically ($\theta = 0^o$ to 180^o) of the cylindrical surface.

The distinguishable feature in heat flux distribution curve over a cylindrical surface is that it shows an initial increasing trend followed successively by a decreasing one and again by an increasing trend. The highest heat flux occurs a little away from the stagnation point, after which, the heat flux decreases with θ due to the growth of the thermal boundary layer in the wall jet region.

The heat flux decreases up to the point of flow separation, after which, it increases further with θ in the wake region of the flame jet. It is found that the peak heat flux shifts away from the stagnation point with a decrease in cylinder diameter.

Therefore, the heat flux is relatively lower for lower values of *D/d* in the stagnation region. Flux distributions with θ are shifted away towards the rear side for higher values of *D/d* due to the delay in flow separation. In case of a diffusion flame, the heat flux in the stagnation region is more than that in a premixed flame (Figs. 8 and 9) while the peak heat flux remains almost identical for both the cases.

Therefore, the heat flux distribution is relatively flat in the stagnation region for diffusion flames. It can be mentioned in this context that the minimum value of local heat flux may be attained either at stagnation point or at separation point depending upon the situation.

For example, in a premixed flame, the minimum value of heat flux for all values of *D/d* occurs at a stagnation point (Fig. 8).

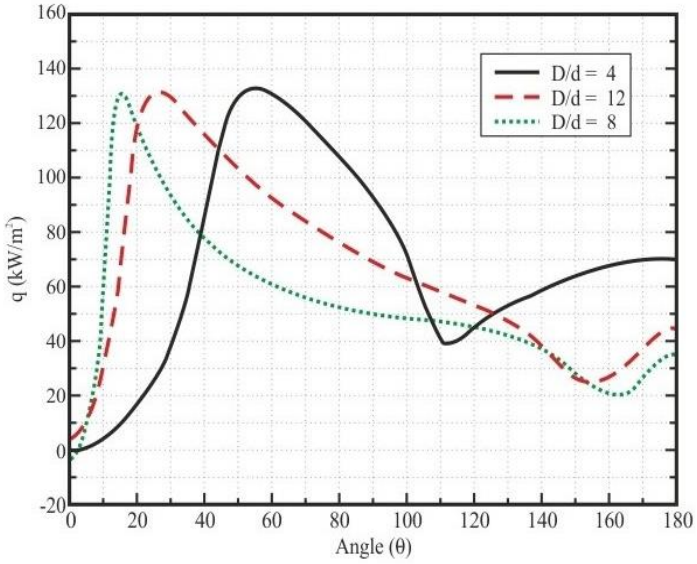

Fig. 8. Distribution of local heat flux for various values of *D/d* in premixed flame at *H/d* = 8, Re = 6000 and ER = 1.

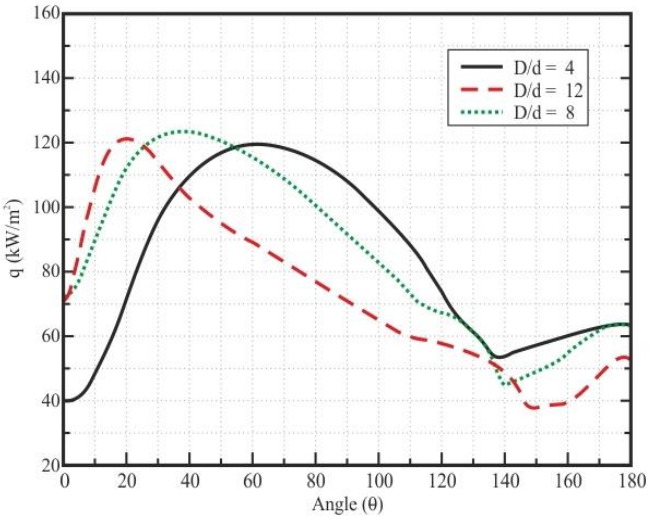

Fig. 9. Distribution of local heat flux for various values of *D/d* in diffusion flame at *H/d* = 8, Re =6000 and ER = 1).

However, it is observed in case of a diffusion flame that the minimum value of local heat flux occurs at the point of separation for *D/d* = 8 and 12 (Fig. 9). In Fig. 10, the point of maximum heat flux corresponds to the point at which, maximum fluid temperature occurs flows to the target plate. Accordingly, at $\theta = 18^0$ the maximum heat flux is obtained for *H/d* = 12. Similarly, the maximum heat flux for *H/d* = 8 and *H/d* = 4 occurs at $\theta = 25^0$ and $\theta = 37^0$ respectively. Thereafter, as the boundary layer thickness increases heat flux decreases continuously. Due to recirculation of flow for *H/d* = 8 from $\theta = 150^0$ to $\theta = 180^0$ the heat flux increases. It is observed from Figs. 10 and 11 that with an increase in *H/d*, the point of maximum heat flux comes closer to the stagnation point in case of both premixed and diffusion flames. This trend is similar to that observed in the case of flame impingement on the plane circular target plate.

Though the maximum value of heat flux remains almost the same for all values of *H/d*, the local heat flux in-wall jet region is relatively higher (Figs. 10 and 11) for higher values of *H/d*. This is in contrast to that found in case of a plane circular target plate. This can be attributed to the coupled effect of flame jet acceleration due to the target surface curvature and the additional turbulence due to large entrainment of air.

Figures 12 and 13 show the surface heat flux distributions for a rich mixture (ER = 2) in case of both premixed and diffusion flames. The heat flux distributions hardly show any difference in the results for ER = 1 and ER = 2 in case of a premixed flame. In case of a diffusion flame with a rich mixture (ER = 2), the local heat flux is reduced with a flat distribution over the surface as compared to that in case of ER = 1 as shown in Fig. 9, but the heat flux in the stagnation point slightly increases. For *D/d*=4 the maximum heat flux occurs at around $\theta = 50^0$, whereas, for *D/d*=12, the maximum heat flux occurs at around $\theta = 15^0$. It happens due to the fact that for *D/d* = 4, there is no complete combustion of fuel before it reaches the cylindrical surface, whereas for *D/d*=12 complete

combustion of a fuel occurs before it reaches the cylindrical surface. Accordingly, the point of maximum heat flux is shifted away from the stagnation point ($\theta = 0^0$) when separation distance decreases. A similar trend occurs for both premixed and diffusion flames for different values of Reynolds numbers and equivalence ratio. The surface heat flux after reaching the maximum value at around $\theta = 30^0$ for D/d= 8, it decreases gradually when the value of θ further increases up to 150^0, and thereafter it increases slightly. At around $\theta = 180^0$, i.e., at the top of the cylinder, the heat transfer from the top hot surface to the cold air occurs, due to which, there is a slight increase in local heat flux near the top surface.

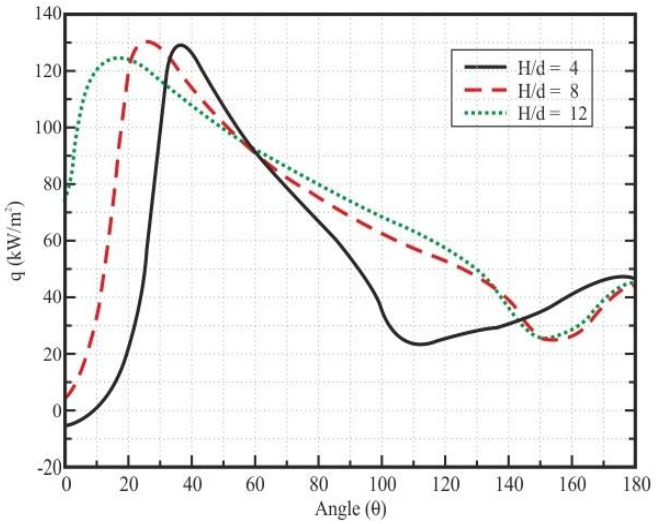

Fig. 10. Distribution of local heat flux for various plate separation distance in premixed flame at *D*/*d* = 8, Re = 6000 and ER = 1.

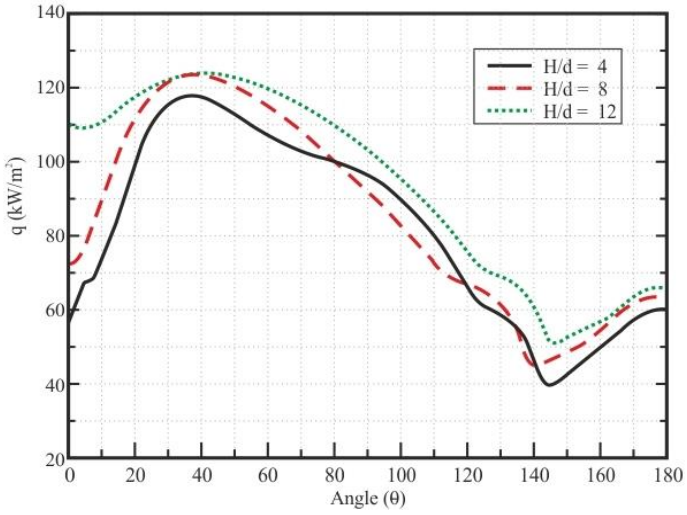

Fig. 11. Distribution of local heat flux for various plate separation distance in diffusion flame at *D*/*d* = 8, Re = 6000 and ER = 1.

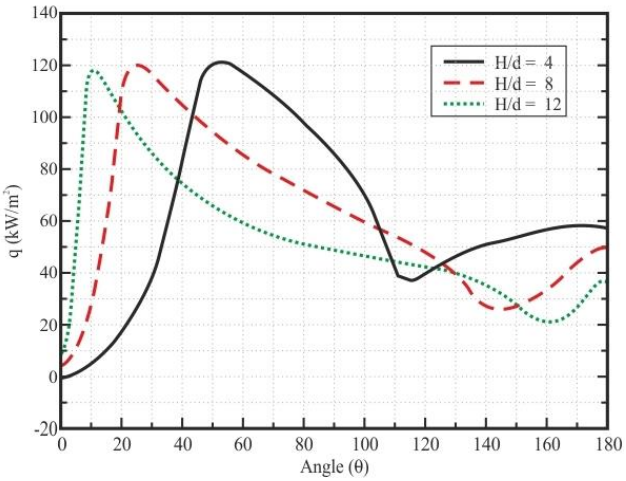

Fig. 12. Distribution of local heat flux for various values of *D*/*d* in premixed flame at *H*/*d* = 8, Re = 6000 and ER = 2).

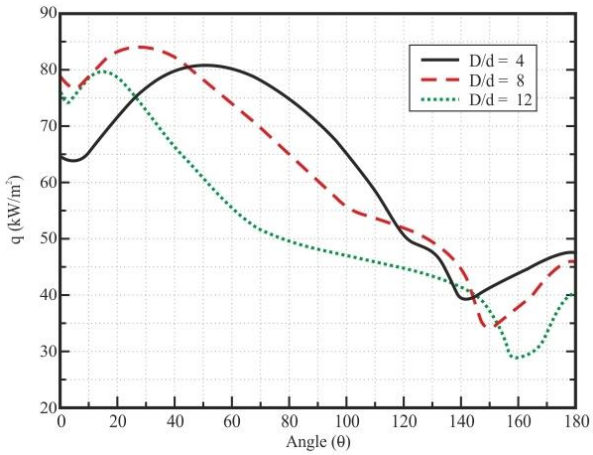

Fig. 13. Distribution of local heat flux for various values of *D*/*d* in diffusion flame at *H*/*d* = 8, Re = 6000 and ER = 2).

4. Conclusions

Premixed and diffusion turbulent flames impinging normally on cylindrical surfaces have been theoretically explored to investigate the influence of geometrical constraints like plate separation distance, Reynolds number, the Equivalence Ratio (ER), etc., on heat transfer characteristics. The significant interpretations made can be summarized as follows:

- The heat flux over the surface of the plate reaches the highest value at a location slightly away from the stagnation region then decreases with radial distance and in the wake region of the flame jet, it further increases.

- With a decrease in cylinder diameter the peak heat flux shifts away from the stagnation region.
- For a lower value of *D/d* the heat flux in the stagnation region is relatively lower.
- Heat flux in the stagnation region is more in diffusion flame than that in premixed flame, while the peak value of heat flux remains almost the same for both the cases.
- When the distance between the plate and the nozzle increases, the peak heat flux comes closer to the stagnation point.
- Though the maximum heat flux remains almost constant for all values of *H/d*, the local heat flux is relatively higher for higher values of *H/d* inside the wall jet region.

Nomenclatures

C_p	Specific heat at constant pressure, kJ/kg K
D	Mass diffusivity, m^2/s
d	Diameter of burner, m
f	Fuel
H	Plate separation height, m
h	Enthalpy, kJ/kg
i	Inlet
K	Thermal conductivity, kW/m.K
M	Molecular weight, kg/k.mol
Nu	Nusselt number
o	Oxidizer
p	Pressure, Pa
q	Heat flux, kW/ m^2
R	Radius of plate, m
Re	Reynolds number
r	Radius of burner, m
r	Radial direction
T	Temperature, K
U	Velocity, m/s
w	Wall
Y	Mass fraction
z	Axial direction

Greek Symbols

α	Thermal diffusivity, m^2/s
γ	Stoichiometric air fuel ratio
ε	Turbulent dissipation rate, m^2/s^3
K	Turbulent kinetic energy, m^2/s^2
μ	Dynamic viscosity, kg/m.s
μ_t	Turbulent viscosity, kg/m.s
ρ	Density, kg/m^3

References

1. Chander, S.; and Ray, A. (2007). Heat transfer characteristics of laminar methane/air flame impinging normal to a cylindrical surface. *Experimental Thermal and Fluid Science*, 32(2), 707-721.
2. Cornaro, C.; Fleischer, A.S.; Rounds, M.; and Goldstein, R.J. (2001). Jet impingement cooling of convex semi-cylindrical surface. *International Journal of Thermal Sciences*, 40(10), 890-898.
3. Dong, L.L.; Cheung, C.S.; and Leung, C.W. (2002). Heat transfer from an impinging premixed butane/air slot flame jet. *International Journal of Heat Mass Transfer*, 45(5), 979-992.
4. Hou, S.-S.; and Ko, Y.-C. (2005). Influence of oblique angle and heating height on flame structure temperature field and efficiency of an impinging laminar jet flame. *Energy Conversion and Management*, 46(6), 941-958.
5. Kuntikana, P.; and Prabhu, S.V. (2016). Isothermal air jet and premixed flame jet impingement Heat transfer characterization and comparison. *International Journal of Thermal Sciences*, 100, 401-415.
6. Agrawal, G.K.; Chakraborty, S.; and Som, S.K. (2010). Heat transfer characteristics of premixed flame impinging upwards to plane surfaces inclined with the flame jet axis. *International Journal of Heat and Mass Transfer*, 53(9-10), 1899-1907.
7. Tripathy, S.; Rout, A.K.; and Roul, M.K. (2016). Heat transfer due to impinging flame on plane surfaces. *International Organization of Scientific Research Journal of Mechanical and Civil Engineering (IOSR-JMCE)*, 13(4), 27-34.
8. Hindasageri, V.; Kuntikana, P.; Vedula, R.P.; and Prabhu, S.V. (2015). An experimental and numerical investigation of heat transfer distribution of perforated plate burner flames impinging on a flat plate. *International Journal of Thermal Science*, 94, 156-169.
9. Wei, Z.L.; Zhen, H.S.; Leung, C.W.; Cheung, C.S.; and Huang, Z.H. (2015). Heat transfer characteristics and the optimized heating distance of laminar premixed biogas hydrogen Bunsen flame impinging on a flat surface. *International Journal of Hydrogen Energy*, 40(45), 15723-15731.
10. Singh, G.; Chander, S.; and Ray, A. (2012). Heat transfer characteristics of natural gas/air swirling flame impinging on a flat surface. *Experimental Thermal and Fluid Science*, 41, 165-176.
11. Nayak, R.C.; Roul, M.K.; and Sarangi, S.K. (2017). Experimental investigation of natural convection heat transfer in heated vertical tubes with discrete rings. *Experimental Techniques*, 41(6), 585-603.
12. Nayak, R.C.; Roul, M.K.; and Sarangi, S.K. (2018). Natural convection heat transfer in heated vertical tubes with internal rings. *Archives of Thermodynamics*, 39(4), 85-111.
13. Sahoo, L.K.; Roul, M.K.; and Swain, R.K. (2017). Natural convection heat transfer augmentation factor with square conductive pin fin arrays. *Journal of Applied Mechanics and Technical Physics*, 58(6), 1115-1122.
14. Sahoo, L.K.; Roul, M.K.; and Swain, R.K. (2018). CFD analysis of natural convection heat transfer augmentation from square conductive horizontal

and inclined pin fin arrays. *International Journal of Ambient Energy*, 39(8), 840-851.

15. Roul, M.K.; and Dash, S.K. (2012). Pressure drop caused by two-phase flow of oil/water emulsions through sudden expansions and contractions: A computational approach. *International Journal of Numerical Methods for Heat and Fluid Flow*, 19(5), 665-688.
16. Roul, M.K.; and Dash, S.K. (2012). Numerical modeling of pressure drop due to single-phase flow of water and two-phase flow of air-water mixtures through thick orifices. *International Journal of Engineering Trends and Technology*, 3(4), 544-551.
17. Gorji-Bandpy, M.; Yahyazadeh-Jelodar, H.; and Khalili, M. (2011). Optimization of heat exchanger network. *Applied Thermal Engineering*, 31(5), 779-784.
18. Pourmehran, O.; Rahimi-Gorji, M.; Gorji-Bandpy, M.; and Baou, M. (2015). Comparison between the volumetric flow rate and pressure distribution for different kinds of sliding thrust bearing. *Propulsion and Power Research*, 4(2), 84-90.
19. Rahimi-Gorji, M.; Ghajar, M.; Kakaee, A.H.; and Ganji, D.D. (2017). Modeling of the air conditions effects on the power and fuel consumption of the SI engine using neural networks and regression. *Journal of the Brazilian Society of Mechanical Sciences and Engineering*, 39(2), 375-384.
20. Magnussen, B.F.; and Hjertager, B.H. (1976). On mathematical models of turbulent combustion with specified emphasis on soot formation and combustion. *Symposium (International) on Combustion*, 16(1), 719-729.
21. van der Meer, T.H. (1991). Stagnation point heat transfer from turbulent low Reynolds number jets and flame jets. *Experimental Thermal and Fluid Science*, 4(1), 115-126.